Smart-fuze Design and Development Based on Computational Analysis of Warhead/Urban-target Interactions

Mica Grujicic[1], William C. Bell

Department of Mechanical Engineering, Clemson University, Clemson, SC 29634, USA

*[1]gmica@clemson.ed

Abstract

Transient non-linear dynamics calculations are carried out to investigate the interactions between a warhead and four different urban targets under different engagement distances and obliquity angles. The results of the calculations are used to guide the design and the development of a smart warhead-fuze which is capable of discriminating between hard targets (e.g. triple-layer brick wall, a light-weight vehicle), soft targets (e.g. an earth and timber bunker), and an urban target (a light-clad domestic building). Robustness of the present approach has been investigated using a statistical sensitivity analysis.

Keywords

Warhead/Urban-target Interaction; Computational Analysis

Introduction

Versatility of weapons such as man-portable, shoulder-launched high energy, dual purpose (HEDP) assault rockets, is essential for infantry preparedness against a wide range of urban targets including: hard targets (e.g. triple brick walls, solid concrete walls, etc.); and soft targets (e.g. sand and timber bunkers, single brick walls, etc.). Until the advent of the MK 420 shock sensing dual mode fuze (Shamblen *et al.*, 1980), the defeat of each target type required a specific warhead design with different pyrotechnic delays. More specifically, a soft target required a pyrotechnic delay (i.e., a delay of explosion) to allow sufficient target penetration prior to detonation, while a hard target required little or no delay, exploding just after initial impact. Without such distinctions, a soft-target warhead would fragment or rupture before the delay had timed out resulting in the loss of explosive and decreased warhead effectiveness, and a hard-target warhead would explode upon impact of a soft target simply marring the surface.

The fully-mechanical MK 420 fuze employed separate firing trains (triggered by pressure and shock of impact deceleration) for hard and soft targets (Shamblen *et al.*, 1980). The hard target firing train responded to mushrooming of the warhead case and the ensuing dynamic pressure increase within the explosive fill. The soft target firing train reacted to less severe deceleration of soft target impaction initiating a pyrotechnic delay allowing for warhead penetration. The fuze functionality relied on the use of a strong and ductile warhead-case for both dynamic-pressure signal transmission and explosive fill containment. In addition, the use of structurally stiff (i.e., fully dense) aluminized composition A-3 explosive for low-loss dynamic pressure transmission was essential.

The mechanical MK 420 fuze for the HEDP assault rocket was eventually replaced by the electromechanical single-mode PZ-11 fuze and the dual-mode PZ-13 fuze equipped with deceleration signal recognition and positive safing features (Koudela, 2007). These fuzes are utilized in the current Shoulder-launched Multipurpose Assault Weapon (SMAW) 83mm High Explosive Dual Purpose (HEDP) warhead. In certain Military Operations in Urban Terrain (MOUT) engagements, it is desirable to have a warhead detonated in the interior of a target structure after having penetrated it, either through its structured ingress points (windows and doors), or through its exterior walls. The current fuzes have limitations in ensuring that a round, after penetrating an urban target structure, will be detonated within its interior, before exiting the structure. It is, hence, desirable to have a fuze which will be able to provide a "void-sensing" mode, in addition to the current hard- and soft-target sensing modes. Such a fuze should be able to sense and differentiate between the initial "thin-wall" shock loading and the immediately-following negligible-deceleration free flight through the

structure interior and be able to trigger the round at an appropriate point within the interior of the structure.

The objective of the present work was to model and simulate warhead/urban-target interactions to support the development of a SMAW tri-mode fuze. The work was limited to the SMAW 83mm HEDP warhead and representative hard, soft, and light clad building targets. Toward that end, warhead/target interaction simulations are performed to create deceleration profiles for a series of warhead/target interaction scenarios over a range of the warhead velocities and obliquity impact angles. The simulation effort also included warhead and target geometrical-model development, projectile/target interaction analysis, and sensitivity analysis (to determine the relative importance of the target and warhead material-model parameters).

The following four targets were considered in the present work: (a) 12"-thick Triple Brick Wall construction as defined in the US Army HEL Technical Memorandum 30-78 (Thein and Coltharp, 1978) and US Army Redstone Technical Test Center Test Procedures 03-56 (Hamlett, 1983); (b) Earth and Timber Bunker construction as defined in US Army HEL Technical Memorandum 30-78 and US Army Redstone Technical Test Center Test Procedure 03-56; (c) and (d) The wall structure and the window structure, respectively, of a small domestic building as defined in STANAG 4536, Appendix 2 to Annex A (Thein and Coltharp, 1997).

The organization of the paper is as follows. In the section "Computational Procedure," geometrical models used to represent the warhead and the four targets are presented first, followed by a brief overview of the non-linear dynamics computational procedure utilized in the present work. The section continues with a summary of the dynamic mechanical models used to represent the behavior of the warhead and target materials under ballistic-impact conditions, and ends with a basic formulation of the warhead/target interaction problem. The results obtained in the present work are presented and discussed next, followed by the main conclusions resulting from the present work.

Computational Procedure

Geometrical Model for the Warhead

At the beginning of the present work, a detailed geometrical CAD model for the warhead was created in Catia V5 from Dassault Systems (2006). The main design characteristics of the warhead incorporated in the model are as follows: (a) aluminum warhead-nose/case; (b) composition A-3 explosive fill bonded with 30wt.% powdered aluminum; (c) an onboard flight data recorder; (d) integrated piezo crystal and accelerometer for shock and deceleration sensing; (e) maraging steel rocket-motor section; (f) fiber-glass composite rocket motor nozzle; and (g) aluminum flight stabilizing fins.

The original geometrical model for the warhead contained 43 parts. To obtain a computationally manageable meshed model of the warhead, the original CAD model was simplified by merging the parts made of the same material, and slight geometry and topography simplifications, while ensuring that the mass distribution was preserved. The final warhead geometrical model consisted of 6 parts with smoothed surfaces allowing for the use of a coarser mesh. This simplified geometrical model was then imported into Hypermesh (a high performance pre-processing program from Altair (Hyperworks, 2006) where a tetrahedral mesh was applied to each part with the implementation of mesh matching across part interfaces. Finally, the model was exported as an *Input Deck* (.k file) for LS-DYNA from Livermore Software Technology Corp. (2006). Finally, the .k file was imported into AUTODYN, a transient non-linear dynamics package from Ansys, Inc. (2006).

The geometrical and the meshed models for the warhead as used in the present work are shown in Figures 1(a)–(b) respectively. The models consist of 6 parts, 4036 nodes, and 11800 four-node solid elements.

Four classes of materials were used in the construction of the warhead computational model: aluminum alloys (of various grades), steel, fiberglass and explosive. Three parts (the nose, the data recorder, and the fins) were constructed of aluminum alloys, one part (the rocket motor section) was constructed of maraging steel, while the rocket nozzle (one part) was made of a fiberglass composite. The explosive (one part) was composed of aluminized RDX A-3.

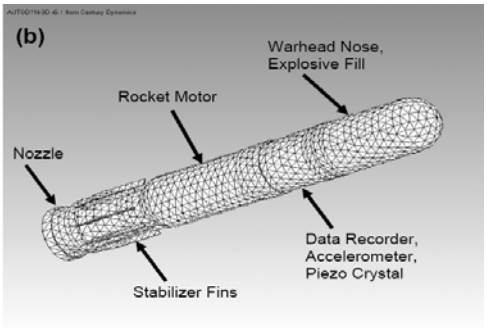

FIG. 1 (A) GEOMETRICAL AND (B) MESHED MODEL FOR THE WARHEAD

Geometrical Model for the Warhead

Upon the completion of the warhead models, the corresponding models for the four targets were generated. A brief description of this procedure is provided in the remainder of this section.

The first urban target analyzed in the present work is a 30cm thick brick wall. The wall is considered to be constructed using standard solid clay masonry facing units (bricks) with the L×W×H dimensions of the brick being 194mm × 89mm × 57mm. The mortar connecting the bricks is a mixture of Type M cementitious material, natural sand aggregate, and water without any admixtures or additives prepared in accordance with the ASTM C270 standard (2007). While the US Army RTTC Test Procedure 03-56 does not mandate the wall dimensions other than thickness (30cm), a wall length of 2.438m in height and 2.439m in length are used in the report example. A standard brick laying pattern as seen in Figure 2 is used. The bottom portion of the wall is assumed to be attached to the ground.

To construct a computational model corresponding to the 30cm-thick triple-brick wall described above, the 3D fragment/brick Lagrange part construction option of AUTODYN was used. This option enables the specification of brick dimensions, mortar thickness, brick lay pattern, wall size and the constituent materials. An example of the computational domain used to represent the 30cm think triple brick wall is shown in Figure 2.

The second urban target analyzed is an earth and timber bunker consisting of sand and timbers that are half submerged in a hole of depth 1.02m and surrounded by a perimeter of stacked sandbags. The 55.8cm wide gap between the timber structure and sandbag perimeter is filled with loose sand. One side of the bunker has an entrance opening, while the opposite side has a firing aperture. Measured from ground level, the bunker dimensions are 2.62m in length, 3.53m in width, and 1.52m in height. Detailed dimensions and diagrams can be found in Appendix D of Thein and Coltharp (1978). The structural timber used is Southern Pine with W×H dimensions of 10.2cm × 10.2cm (4in × 4in) or 15.2cm × 15.2cm (6in × 6in) depending on which is available. After the timber structure has been built and placed in the hole, the sandbags are placed to form double rows laid parallel to the perimeter, alternating with single rows laid perpendicular to the perimeter.

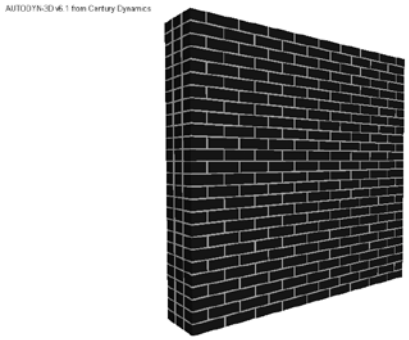

FIG. 2 COMPUTATIONAL MODEL FOR THE TRIPLE LAYER BRICK WALL

In order to construct a computational model of the earth and timber bunker, a single three-layer side wall was selected, using only the aboveground portion. The computational wall consists of the double row of sandbags, loose sand, and the pine-timber structure. The sand bags were created using six-sided closed-shell parts. Each part was then given a minimal shell thickness to represent the plastic bag thickness. These closed-shells parts were then filled with the loose sand material from the AUTODYN material model database. The loose sand layer was then given the dimensions detailed in appendix D-7 of Thein and Coltharp (1978) and was also filled with the loose sand material from the AUTODYN material model database. Finally, the pine-timber wall was constructed using a single 3D Lagrange block-shape part with a 10.2cm thickness and a specifically developed pine timber material model. These three layers were all connected using the part joining feature within AUTODYN. An example of the computational domain used to represent the earth and timber bunker is shown in Figure 3.

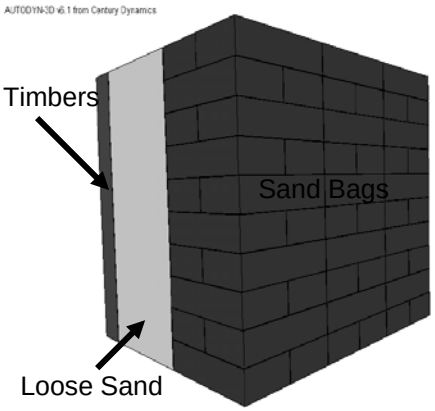

FIG. 3 COMPUTATIONAL MODEL FOR THE EARTH AND TIMBER BUNKER

The final urban target to be analyzed is the small domestic building with two windows and one door. Two impact test points within this structure were

analysed: (a) the solid wall structure; and (b) the window structure. The solid wall structure was created using a two layer wall. The outer wall is made of solid lightweight concrete blocks with nominal dimensions of 440mm × 215mm × 190mm and a mortar thickness of 15mm. A standard half block-length laying stagger is used in the outer wall construction. The inner wall is constructed using hollow bricks with nominal dimensions of 500mm × 200mm × 100mm and a mortar thickness of 15mm. A standard half brick-length laying stagger is used in the inner wall construction. The window is a standard wood framed window of dimensions 1.2m × 1.4m.

The computational models of the solid wall structure and the window structure were constructed separately within AUTODYN. To construct the computational model of the solid wall target, the outer wall was first created using a 3D fragment/brick Lagrange part with the dimensions, mortar thickness, and block laying pattern discussed above. Then, the concrete material model from the AUTODYN material database and the mortar material model were applied. Next, the computational model of the hollow-brick inner wall of the solid wall structure was constructed also using a 3D fragment/brick Lagrange part option. However, since this option allows the construction of only solid-brick walls, the following procedure was applied to construct the needed hollow brick wall. Firstly, each hollow brick is considered to consist of five distinct layers in order to account for the hollow brick architecture. Three of the layers (the two outer layers and the middle layer) are made of clay material while the remaining two layers are predominately void layers. The two outer layers and the middle layer are 20mm-thick walls with brick height and length described above and were created using a 3D fragment/brick Lagrange part. The brick material model and the mortar material described above were applied to their respective sections of the three layers. The remaining two layers were also created using a 3D fragment/brick Lagrange part with the same dimensions, but brick material model was replaced with a void material and the mortar material model was replaced with the brick material model. The five layers of wall are then joined using the AUTODYN part joining feature in order to integrate them into a single wall. The inner and the outer wall were then offset with a small displacement in order to satisfy the AUTODYN gap requirements of non-joined parts. An example of the computational domain used to represent the small domestic building solid wall structure is shown in Figure 4. To construct the computational model for the window structure, a Lagrange block part of the dimensions stated in Appendix 2 to Annex A of Thein and Coltharp (1997) was created. Then the glass material model from the AUTODYN material database was applied to the computational domain. An example of the computational domain used to represent the small domestic building window structure is shown in Figure 5.

Modeling of Warhead/Target Interactions

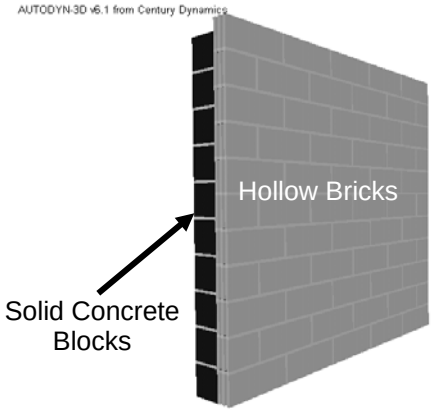

FIG. 4 COMPUTATIONAL MODEL FOR THE SMALL DOMESTIC BUILDING SOLID WALL STRUCTURE

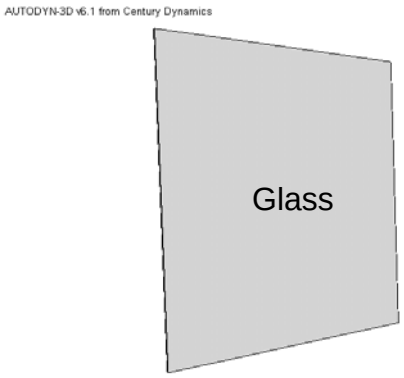

FIG. 5 COMPUTATIONAL MODEL FOR THE SMALL DOMESTIC BUILDING WINDOW STRUCTURE

Computational analyses of warhead/target interactions have been performed, in the present work, using AUTODYN, a general-purpose transient non-linear dynamics modeling and simulation software (Ansys, Inc., 2006). Within AUTODYN, the appropriate mass, momentum and energy conservation equations are combined with the attendant material-model equations and the

appropriate initial and boundary conditions and solved numerically using a second-order accurate explicit scheme. The numerical framework (i.e. the "processor" as referred to in AUTODYN) used is generally dependent on the physical nature of the problem being studied and, for multi-domain problems, different domains can be analyzed using different processors. The Lagrange processor or the SPH (Smooth Particle Hydrodynamics) processor is typically used for solid-continuum structures, while the Euler processor is commonly used for modeling gases, liquids or solids undergoing large deformations and density changes. The Lagrange-based Shell and Beam processors are designated for modeling shell- and beam-like solid structures, respectively. In the present work, the warhead/target interactions were analyzed using the Lagrange processors both for the warhead and the targets. The interactions between the warhead and the target are accounted for through the use of the sub-domain interaction options within AUTODYN (Ansys, Inc., 2006) which were overviewed in detail in our recent work (Grujicic *et al.*, 2007a,b, 2009a,b). Also, a detailed discussion regarding the effect of the processor choice (Lagrange vs. SPH) for the warhead and the target on the computational results can be found in our work (Grujicic *et al.*, 2008 a,b,c, d, 2009c, 2012 a, b, c).

Dynamic Material Models

The complete formulation of a transient non-linear dynamics problem involving impact of a target by the warhead entails the knowledge of materials models (material-specific relations between pressure, stress, mass density, strain, strain rate, internal energy density, etc.). These relations typically involve: (a) an equation of state; (b) a strength equation; (c) a failure equation and (d) an erosion equation for each constituent material. The equation of state defines pressure-dependence on mass density and internal-energy density (and, in the case of anisotropic materials, on deviatoric strain.) The strength and failure equations define the evolutions of the deviatoric stress in the elastic regime, elastic-plastic regime, and in the post failure initiation regime. In other words, the equation of state along with the strength and failure equations enables assessment of the evolution of the complete stress tensor during a transient non-linear dynamics analysis. Such an assessment is needed where the governing conservation equations are being solved. The erosion equation is generally intended for eliminating numerical solution difficulties arising from highly disordered Lagrangian cells. Nevertheless, the erosion equation is often used to provide an additional material failure mechanism especially in materials with limited ductility. When a computational/material cell is eroded, the freed nodes are retained along with their velocities in order to conserve momentum of the system. A summary of the materials and their models used in the construction of the warhead and the four targets is provided in Tables 1 and 2, respectively.

Interaction Problem Definition

TABLE 1 MATERIAL MODELS USED IN VARIOUS COMPONENTS OF THE WARHEAD. PLEASE NOTE THAT NO FAILURE EQUATION IS AVAILABLE FOR ANY MATERIAL.

Component	Material	EOS	Strength	Erosion
Nose	Al 2024	Shock	Steinburg Guinan	Geom. Strain
Explosive	Aluminized RDX A-3	Porous	von Mises	Geom. Strain
Recorder Section	Al 6061-T6	Shock	Steinburg Guinan	Geom. Strain
Fins	Al 7075	Shock	Steinburg Guinan	Geom. Strain
Rocket Motor	Maraging Steel	Linear	Johnson Cook	Geom. Strain
Nozzle	Fiberglass Composite	Rigid	N/A	Geom. Strain

TABLE 2 MATERIAL MODELS USED IN THE FOUR TARGETS

Material	EOS	Strength	Failure	Erosion
Brick	Porous	Drucker-Prager	Hydro(Pmin)	Geom. Strain
Mortar	Porous	Drucker-Prager	Hydro(Pmin)	Geom. Strain
Sand	Compaction	MO Granular	Hydro(Pmin)	Geom. Strain
Timber	Ortho	von Mises	Material Stress/Strain	Geom. Strain
Concrete	P alpha	RHT Concrete	RHT Concrete	Geom. Strain

In the present work, the transient non-linear dynamics analyses of the impact (and in the case of soft and domestic-building targets, the penetration) of the targets by the warhead are carried out in order to determine the temporal evolutions of the warhead velocity (as measured at the location of the accelerometer) and dynamic load (as measured by the piezo crystal). Due to the presence of discrete non-axisymmetric fins and other flight recorder components and since the warhead/targets interactions are analyzed under different obliquity impact angles, full 3D analyses had to be carried out. Examples of the warhead/hard-target warhead/soft-target and impact/penetration problems analyzed here

are given in Figures 6 and 7, respectively. A constant initial normal velocity of in a 150-300m/s range is assigned to all six parts of the warhead.

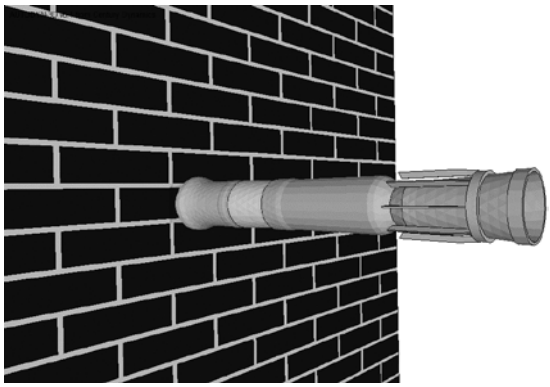

FIG. 6 WARHEAD/HARD-TARGET INTERACTION

Since both the warhead and the targets were represented using Lagrange processors, the warhead/target interactions were accounted for using the Lagrange/Lagrange part-coupling option available in AUTODYN. Except for the warhead/target contact surfaces, zero-stress boundary conditions were prescribed on all faces of the warhead and front and back faces of the targets.

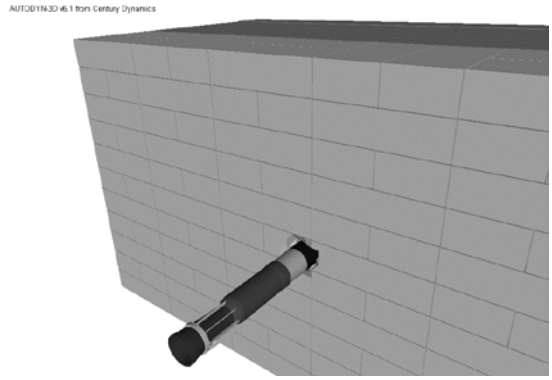

FIG. 7 WARHEAD/SOFT-TARGET INTERACTION

To mitigate the effect of reduced-size of the target models and to simulate the effect of the surrounding frame structure, "transmit" boundary conditions were applied to the top and side faces of the targets. The transmit boundary conditions enable the propagation of pressure waves across the boundaries without reflection mimicking wave propagation in an infinitely-large domain (Ansys, Inc., 2006). To account for the fact that the bottom portion of the three-layer brick wall is attached to the ground, transmit and "zero-velocity" boundary conditions were applied to the bottom face of this target. Likewise, to account for the buried section of the wall and the other connecting walls of the earth and timber bunker, transmit and zero-velocity boundary conditions were placed on all four lateral faces of this target. The zero-velocity boundary conditions also ensured that the loose-sand layer would remain contained as it would be the case in the full structure. In the case of the domestic-building wall, transmit and zero-velocity boundary conditions were applied on all four side faces of the structure, in order to account for the connection of this wall to the rest of the building. Similarly, transmit and zero-velocity boundary conditions were applied on all four sides of the glass structure.

To improve the accuracy of the analysis, smaller cells were used in the regions of the warhead and the targets involved in the warhead/target interactions. A standard mesh sensitivity analysis was carried out in order to ensure that the results obtained are essentially insensitive to a further refinement in the cell size.

Results and Discussion

Typical Warhead/Target Impact Results

As mentioned earlier, the main purpose of the transient non-linear dynamics calculations of the warhead/target interactions was determination of the temporal evolution of the warhead velocity (at the location of its accelerometer) and the dynamic load (at the location of the piezo crystal). Such temporal evolutions are determined as a function of the initial (impact) warhead speed and the obliquity (impact) angle for each of the four targets. Details of the results obtained can not be disclosed here due to potential for their misuse. Instead, only typical qualitative results will be presented.

An example of the results pertaining to the temporal evolution of the warhead velocity in the case of the hard and the soft targets is shown in Figure 8 (a). In addition, the temporal evolution of the depth of penetration of the soft target is displayed in Figure 8 (b). (It should be noted that no penetration of the hard target takes place and the result of the warhead/hard-target interaction is minor damage to the strike face of the target and large-scale damage to the warhead nose.)

An example of the results pertaining to the temporal evolution of the dynamic loads in the case of the hard and soft targets is shown in Figure 9. It should be noted that in order to improve clarity, the two dynamic-load traces displayed in Figure 9 are offset in the vertical direction. Also, the results displayed in

Figure 9 are further processed using a discrete Fourier-transform based signal-processing algorithm in order to identify the main harmonics in the dynamic-loading signal.

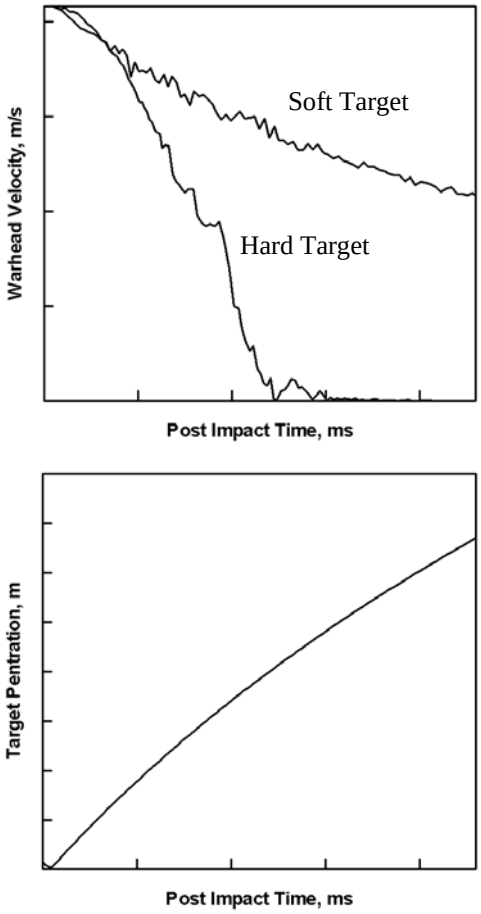

FIG. 8 (A) TEMPORAL EVOLUTIONS OF THE WARHEAD VELOCITY FOLLOWING IMPACT WITH A HARD AND SOFT TARGET; (B) TEMPORAL EVOLUTION OF THE SOFT-TARGET PENETRATION BY THE WARHEAD

As mentioned earlier, the results like the ones displayed in the Figures 8 and 9 are used to guide design and development of a triple-mode warhead fuze which will be able to recognize different (structural) targets (i.e. a hard, a soft or a light clad domestic building target and activate the appropriate pyrotechnical delay.) In such a process, various components of the results (e.g. the maximum deceleration at the post-impact time at which such deceleration takes places in the case of the hard target, or the residual warhead velocity in the case of the domestic building targets) are used. In addition to the computational results presented here, the fuze design and development is also guided using the corresponding experimental results obtained from a companion experimental program which involves the investigation of number of test structures. Such experimental studies are critical for ensuring the validity of the warhead/ target computational analysis presented in the present work. Further validation of the computational procedures discussed here is presented in next section, where the aspects of the robustness (i.e. statistical sensitivity of the computational results to changes in the material model parameters) are discussed.

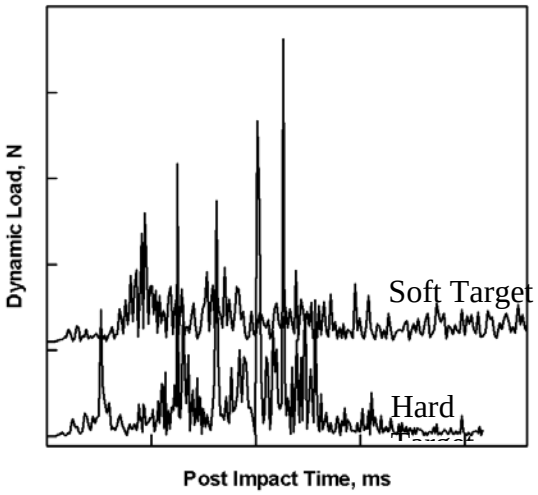

FIG. 9 TEMPORAL EVOLUTIONS OF THE DYNAMIC LOADS EXPERIENCED BY THE PIEZO CRYSTAL LOCATED IN THE FLIGHT-RECORDER SECTION OF THE WARHEAD.

Statistical Sensitivity Analysis

As discussed earlier, the computational results obtained in the present work, which pertain to the temporal evolutions of warhead velocity and dynamic loads during warhead/target interactions, are used to guide the design and development of a fuze which can discriminate between different types of targets and activate the corresponding pyrotechnic delay mechanism. In the present work, the material models available in the AUTODYN material database and a few materials developed as a part of the present work (e.g. aluminized composition A3, mortar, etc) were used. These models were derived initially using a combination of the experimental investigations and phenomenological correlation analyses. Consequently, the values of material-model parameters contain some uncertainty and it is critical to assess how the potential errors associated with these parameters may affect the results of the computational analyses. To tackle this problem, the standard statistical sensitivity analysis is employed. In addition, to make the computational problem manageable, a design of experiments (DOE) approach was used to reduce the number of computational analyses, needed to carry out the

statistical analysis. Since the statistical sensitivity analysis and the DOE are fairly well known concepts, they will be reviewed here only briefly.

The DOE is a systematic approach for the investigation of a system or process. A series of structured tests are designed in which changes are made to the input variables (factors) of the system/process and the effects of these changes on a pre-defined output (objective function) are assessed. The DOE is a formal way of maximizing the information gained per amount of effort/ resources used.

Statistical sensitivity analysis enables identification of the main contributing factor(s) to the problem. The first step in the statistical sensitivity analysis is identification of the relevant factors and their ranges of variation. Within such ranges, 2-4 (3 in the present work) levels of each factor are identified.

In the present work, one level (level 2) of each factor is taken to correspond to the values of the mean material model parameters as defined in the AUTODYN material database. The other two levels of the factors correspond to the values of the material parameters decreased (level 1) or increased (level 3) by one standard deviation. An example of a statistical sensitivity analysis in which four factors were used (along with their levels) is given in Table 3. It should be noted, the levels of the four factors listed in Table 3 have been normalized with respect to the corresponding mean values.

The next step in the statistical sensitivity analysis is to identify the number and the type of the computational procedures (the transient non-linear dynamics analyses in the present work) which need to be performed in order to quantify the effect of the selected factors. A factorial-design approach is available within which all possible combinations of the factor levels are used. However, the number of the analyses to be carried out can quickly become unacceptably large as the number of factors and levels increases. For the case shown in Table 3, 81 ($=3^4$) analyses would have to be performed according to the full factorial approach. To reduce the number of analyses, the orthogonal matrix method (Montgomery, 2002) was used in which a separate column is allocated to each factor, while each row represents a particular combination of the levels for each factor. Thus, the number of analyses which needs to be performed is equal to the number of rows of the corresponding orthogonal matrix. The columns of the matrix are mutually orthogonal, that is, for any pair of columns, all combinations of the levels of the two associated factors appear and each combination appears an equal number of times. A limited number of standard orthogonal matrices (Ross, 1996) are available to accommodate specific numbers of the factors with various numbers of levels per factor. For the four-factor/three-level case, the L_{18} 3^4 orthogonal matrix is used which defines 18 computational analyses which have to be performed. The factor levels associated with each of these analyses is given in Table 4.

TABLE 3 STATISTICAL SENSITIVITY ANALYSIS FACTORS AND LEVELS USED IN THE PRESENT WORK

Factors	Levels		
	1	2	3
Compressive Strength (A)	0.80	1.0	1.2
Damage Exponent (B)	0.80	1.0	1.2
Compaction Exponent (C)	0.80	1.0	1.2
Erosion Strain (D)	0.80	1.0	1.2

A computational transient non-linear dynamics analysis is next performed for each combination of the factor levels as defined in the appropriate row of the orthogonal matrix. The values of the objective function (e.g., warhead time-to-full- stop in the case of the hard target, depth of penetration of the target after a predefined post impact delay time in the case of a soft target, and residual velocity in the safe of a domestic building target) resulting from each of the 18 analyses are next displayed in Table 4, along with the mean value of the objective function. It should be noted that the analysis 2 in Table 4, for which all four factors are set to their mean value (level 2).

The mean values of the objective function associated with each of the three levels of each of the four factors are next calculated. This is done by averaging the values of the objective function associated with a specific level of a given factor. The results of this calculation are given in Table 5. The effect of a level of a factor is then defined as the deviation caused from the overall mean value and thus obtained by subtracting the overall mean value from the mean value associated with the particular level of that factor. This process of estimating the effect of factor levels is generally referred to as the "Analysis of Means" (ANOM). The ANOM allows determination of the

main effect of each factor. However, using this procedure, it is not possible to identify possible interactions between the factors.

TABLE 4 L_{18} (3^4) ORTHOGONAL MATRIX USED IN THE STATISTICAL SENSITIVITY ANALYSIS

Analysis Number	Levels				Objective Function
	Factor A	Factor B	Factor C	Factor D	
1	1	1	1	1	20.749
2	2	2	2	2	21.876
3	3	3	3	3	21.854
4	1	1	2	2	21.224
5	2	2	3	3	22.288
6	3	3	1	1	20.989
7	1	2	1	3	22.301
8	2	3	2	1	21.733
9	3	1	3	2	21.968
10	1	3	3	2	22.531
11	2	1	1	3	20.795
12	3	2	2	1	21.111
13	1	2	3	1	21.482
14	2	3	1	2	21.751
15	3	1	2	3	21.907
16	1	3	2	3	22.186
17	2	1	3	1	21.526
18	3	2	1	2	21.018
Overall Mean of the Objective Function					21.627

TABLE 5. AN EXAMPLE OF THE RESULTS OBTAINED IN THE ANOVA STATISTICAL SENSITIVITY ANALYSIS

Factor	Difference From Mean, (m/s)			Sum of Squares $(m/s)^2$	Percent of Sum of Squares	Number of D.O.F	Variance Ratio F
	Level 1	Level 2	Level 3				
A	0.088	0.025	0.113	0.127	4.561	2	0.705
B	0.197	0.039	0.158	0.392	14.11	2	2.181
C	0.267	0.034	0.233	0.760	27.34	2	4.226
D	0.269	0.075	0.194	0.692	24.88	2	3.846
Error	N/A			0.810	29.11	9	1.000
	Total			2.781	100.0	N/A	N/A

To obtain a more accurate indication of the relative importance of the factors and their interactions, the *"Analysis of Variance"* (ANOVA) is used. The ANOVA allows determination of the contribution of each factor to the total variation from the overall mean value. This contribution is computed following the procedure which was presented in a step-by-step fashion, in our previous work. Consequently, the implementation details for the procedure will not be discussed here. The final outcome of the ANOVA is a list of values for the variance ratio, F, which are listed in the last column of Table 5. F is used to quantify the absolute and the relative magnitude of the effect of each factor for a given level of confidence. A value of F less than F_{crit} (dependent on the level of confidence), implies that the effect of the corresponding factor is smaller than the error (arising from a linear-superposition approximation) and, hence, the interaction of the factor in question with other factors can be ignored. A value of $F > F_{crit}$ implies the otherwise.

The results displayed in Table 5 should be interpreted as follows. Based on the results given in Column 6 *"Percent of sum of squares"* the four factors should be ranked (in ascending order) relative to their effect on the objective function as: *ABDC*. Furthermore, based on the results presented in the last column *"Variance Ratio"* and using a 90% confidence level (F_{crit} = 3.01), the factor whose effect is dependent the most on the levels of the other factors are factors, *C* and *D*. This implies that the material model parameters corresponding to the factors *C* and *D* have to be determined with the highest accuracy, since the results of the computational analyses are most effected by variations of these two factors.

Summary and Conclusions

In the present work, a brief overview is presented of the computational procedure used to guide the design and development of a triple-mode fuze for shoulder-launched multi-purpose assault weapon warheads. Such a fuze is required to recognize the type of urban target (e.g. a triple-layer brick wall, a light concrete wall, a glass pane etc.) and to actuate the appropriate pyrotechnic delay needed to achieve the maximum effectiveness of the warhead.

REFERENCES

ASTM C270-07 Standard Specification for Mortar for Unit Masonry, 2007.

AUTODYN-2D and 3D, Version 6.1, User Documentation, Ansys, Inc., 2006.

CATIA, Version 5 Revision 17, Dassault Systèmes, 2006.

Grujicic, M., Pandurangan, B., Angstadt, D., Koudela, K., and Cheeseman, B.A., "Ballistic-Performance

Optimization of a Hybrid Carbon-Nanotube/E-glass Reinforced Poly-Vinyl-Ester-Epoxy-Matrix Composite Armor," Journal of Materials Science, 42(2007a):5347–5359.

Grujicic, M., Pandurangan, B., Zecevic, U., Koudela, K. L. and Cheeseman, B. A., "Ballistic Performance of Alumina/S-2 Glass-Reinforced Polymer-Matrix Composite Hybrid Lightweight Armor Against Armor Piercing (AP) and Non-AP Projectiles", Multidiscipline Modeling in Materials and Structures, 3(2007b): 287–312.

Grujicic, M., Bell, W. C., Thompson, L. L., Koudela, K. L. and Cheeseman, B. A., "Ballistic-Protection Performance of Carbon-Nanotube Doped Poly-Vinyl-Ester-Epoxy Composite Armor Reinforced with E-glass Fiber Mats", Materials Science and Engineering A, 479(2008a): 10–22.

Grujicic, M., Bell, W. C., Biggers, S. B., Koudela, K. L. and Cheeseman, B. A., "Enhancement of the Ballistic-Protection Performance of E-glass Reinforced Poly-Vinyl-Ester-Epoxy Composite Armor via the Use of a Carbon-Nanotube Forest-Mat Strike Face", Journal of Materials: Design and Applications, 222(2008b): 15–28.

Grujicic, M., Arakere, G., He, T., Gogulapati, M. and Cheeseman, B. A., "A Numerical Investigation of the Influence of Yarn-Level Finite-Element Model on Energy Absorption by a Flexible-fabric Armor During Ballistic Impact", Journal of Materials: Design and Applications, 222(2008c): 259–276.

Grujicic, M., Arakere, G., He, T., Bell, W. C., Cheeseman, B. A., Yen, C.-F. and Scott, B., "A Ballistic Material Model for Cross-Plied Unidirectional Ultra-High Molecular Weight Polyethylene Fiber-Reinforced Armor-Grade Composites", Materials Science and Engineering A, 498 (2008d): 231–241.

Grujicic, M., Arakere, G., He, T., Bell, W. C., Glomski, P. S., Cheeseman, B. A., "Multi-scale Ballistic Material Modeling of Cross-plied Compliant Composites", Composites Part B: Engineering, 40(2009a): 468–482.

Grujicic, M., Glomski, P. S., He, T., Arakere, G., Bell, W. C., Cheeseman, B. A., "Material Modeling and Ballistic-resistance Analysis of Armor-Grade Composites Reinforced with High-Performance Fibers," Journal of Materials Engineering and Performance, 18(2009b): 1169–1182.

Grujicic, M., Bell, W. C., Arakere, G., He, T. and Cheeseman, B. A., "A Meso-Scale Unit-Cell Based Material Model for the Single-ply Flexible-Fabric Armor," Materials and Design, 30(2009c): 3690–3704.

Grujicic, M., Pandurangan, B., d'Entremont, B. P., Yen, C.-F. and Cheeseman, B. A., "The Role of Adhesive in the Ballistic/Structural Performance of Ceramic/Polymer-Matrix Composite Hybrid Armor", Materials and Design, 41(2012a): 380–393.

Grujicic, M., Pandurangan, B., and Coutris, N., "A Computational Investigation of the Multi-Hit Ballistic-Protection Performance of Laminated Transparent Armor Systems", Journal of Materials Engineering and Performance, 21(2012b): 837–848.

Grujicic, M., Bell, W. C. and Pandurangan, B., "Design and Material Selection Guidelines and Strategies for Transparent Armor Systems", Journal of Materials and Design, 34(2012c): 809–819.

Hamlett, T., "RTTC Procedures for the Construction of the MOUT Target Set", Redstone Technical Test Center, March 2003.

Hyperworks, Version 7.0, Altair Engineering, Inc., 2006.

Koudela, K.L, Pennsylvania State University, private communication, March 22, 2007.

LS-DYNA, Livermore Software Technology Corp., 2006.

Montgomery, D.C. Design and Analysis of Experiments. Hoboken, NJ: Wiley Publishers, 2002.

Ross, P. J. Taguchi Techniques for Quality Engineering: Loss Function, Orthogonal Experiments, Parameter and Tolerance Design, Second Edition. New York, NY: McGraw-Hill, 1996.

Shamblen, M., Walchak, M. and Richmond, L., "Shock Sensing Dual Mode Warhead", U.S. Patent 5591935, August 1980.

Thein, B. and Coltharp, D., "Interim Standards for the Construction of MOBA Structures for Weapons Effects Tests", US Army Technical Memorandum 30–78, December 1978.

Thein, B. and Coltharp, D., "STANAG 4536 on Representative Building Targets, Unfortified and Fortified", Military Agency for Standardization, November 1997.